Modeling post-logging height growth of black spruce-dominated boreal forests by combining airborne LiDAR and time since harvest maps

Batistin Bour[1], Victor Danneyrolles[1]*, Yan Boucher[2, 3], Richard A. Fournier[1] and Luc Guindon[4]

[1] Département de Géomatique appliquée, Centre d'Application et de Recherche en Télédétection (CARTEL), Université de Sherbrooke, 2500 Boulevard de l'Université, Sherbrooke, QC JIK 2R1, Canada

[2] Département des Sciences Fondamentales, Laboratoire d'écologie végétale et animale, Université du Québec à Chicoutimi, 555 boulevard de l'Université, Chicoutimi, QC G7H 2B1, Canada

[3] Direction de la Recherche Forestière, Ministère des Forêt, de la Faune et des Parcs du Québec, 2700 rue Einstein, Québec, QC G1P 3W8, Canada

[4] Natural Resources Canada, Canadian Forest Service, Laurentian Forestry Centre, 1055 du P.E.P.S., St. Sainte-Foy, P.O. Box 10380, Québec, QC G1V 4C7, Canada

*Corresponding author: Victor Danneyrolles, victor.danneyrolles@usherbrooke.ca

Abstract

Increase in forest disturbance due to land use as well as climate change has led to an expansion of young forests worldwide, which drives global carbon dynamics and timber allocation. This study presents a method that combines a single airborne LiDAR acquisition and time since harvest maps to model height growth of post-logged black spruce-dominated forests in a 1700 km^2 eastern Canadian boreal landscape. We developed a random forest model where forest height at a 20 m × 20 m pixel resolution is a function of stand age, combined with environmental variables (e.g., slope, site moisture, surface deposit). Our results highlight the model's strong predictive power: least-square regression between predicted and observed height of our validation dataset was very close to the 1:1 relation and strongly supported by validation metrics (R^2 = 0.74; relative RMSE = 19%). Environmental variables thus allowed to accurately predict forest productivity with a high spatial resolution (20 m × 20 m pixels) and predicted forest height growth in the first 50 years after logging ranged between 16 and 27 $cm.year^{-1}$ across the whole study area, with a mean of 20.5 $cm.year^{-1}$. The spatial patterns of potential height growth were strongly linked to the effect of topographical variables, with better growth rates on mesic slopes compared to poorly drained soils. Such models could have key implications in forest management, for example to maintain forest ecosystem services by adjusting the harvesting rates depending on forest productivity across the landscapes.

Key words: Natural forest regrowth, remote sensing, airborne LiDAR, forestry practices, land-use, carbon mitigation, landscape changes.

Introduction

Over the last few decades, an increase in forest disturbance due to land use as well as climate change has led to the expansion of young forests worldwide (McDowell et al. 2020). This trend is likely to continue or even increase in the future (Boucher et al. 2017, McDowell et al. 2020). Thus, these young forests are playing an increasing and critical role in a variety of issues, for example, reaching a balance in global carbon dynamics (Cook-Patton et al. 2020) and maintaining forest ecosystem services. These regenerating forests represent a critical stage in subsequent successional dynamics (Lindenmayer et al. 2019) and generally exhibit the highest growth rate patterns. Yet, the dynamics of young forests have received surprisingly much less attention than have mature or old growth forests. More specifically, greater insights and better methods for modeling forest growth at such early stages of succession would considerably improve our ability to predict and manage changes in these forest landscapes.

Several factors may control young forest growth dynamics. For one, the time that has elapsed since the last stand-replacing disturbance (e.g., clearcutting, fire) plays an important role. Forest height follows a sigmoid pattern over time: growth rates are generally maximal in the early stages of succession and tend to decline progressively with stand age as the trees attain their maximum height (Ryan et al. 2004). Yet, forest height growth is also mediated by a combination of environmental gradients operating at several scales. Regional climate plays an important role through three potential limiting factors: light, temperature and water (Boisvenue and Running 2006, Cook-Patton et al. 2020). In boreal forests, temperature is the main climatic limiting factor for growth with a short growing season (Huang et al. 2010), followed by regional drought events (D'Orangeville et al. 2018). Climatic gradients are also mediated by landscape-scale topographic gradients. For example, altitude, slope and exposure generate a diversity of local temperature characteristics that can influence the growth rates at the landscape scale (Nicklen et al. 2016). Similarly, site moisture conditions are strongly mediated by topography, surface deposits and drainage, with mesic mid- and upper-slopes generally leading to better tree growth rates when compared to poorly drained soils at lower slope positions (Lavoie et al. 2007, Laamrani et al. 2014).

There is an important and persistent tradition in ecology and forestry for the development of forest growth models (e.g., Vanclay and Skovsgaard 1997, Weiskittel et al. 2011). Currently, most models are based on data gathered from extensive field measurements, such as long-term permanent plot networks (e.g., Pretzsch et al. 2014), or dendrochronological analyses of large numbers of trees (e.g., Huang et al. 2010, D'Orangeville et al. 2018). While acquisition of these data is generally time-consuming and expensive, the development of remote sensing methods to estimate forest structure characteristics offers cheaper alternatives, more specifically with respect to Light Detection And Ranging (LiDAR) (e.g., Næsset et al. 2013). Several studies have already proposed modeling forest growth using repeated airborne LiDAR acquisition (e.g., Meyer et al. 2013, Cao et al. 2016, Tompalski et al. 2021). Yet, these repeated acquisitions remain rather time-consuming and expensive since they imply a relevant time lapse between surveys (e.g., 5 to 10 years), which may further imply methodical challenges due to potential changes in LiDAR technological characteristics between surveys. As an alternative to repeated acquisitions, some studies have proposed to combine a single LiDAR acquisition with estimated time-since-disturbance spatial data to model forest growth or productivity (Lefsky et al. 2005, Pflugmacher et al. 2014, Tompalski et al. 2015). These growth models can have key implications in forest management. For example, Tompalski et al. (2015) used this approach to identify forest site productivity classes across the landscape. Such outcomes may help the forest industry determine the sustainable harvesting rates that maintain forest ecosystem services such as carbon sequestration.

In this study, we used this simple approach combining a single airborne LiDAR acquisition with stand age (assessed from historical time since harvest maps) to model forest height growth of post-logged boreal forests that are dominated by black spruce (*Picea mariana* [Mill.] BSP). Most sustainably managed forest landscapes include such time since harvest maps, particularly in even-aged managed stands (i.e., managed mostly through stand-replacing clearcuts). Our first objective was to develop and evaluate a predictive model of young forest stand height (10 to 50 years) as a function of stand age and other environmental key determinants (e.g., slope, site moisture, surface deposits). The second objective was to use these environmental determinants of forest growth to predict forest productivity across the landscape. We finally discuss the potential implications of our results for forest management.

Materials and methods

Study area

The study area covers 1,700 km^2 in the closed-crown boreal forests in the North Shore region of Quebec, eastern Canada (Fig. 1). Elevation ranges between 125 and 700 m and is associated with an important topographical gradient that includes lowlands and highland plateaus, and slopes that range between 0 and 20 degrees. The climate is typical of eastern Canadian boreal forest, with cold mean annual temperatures (-2.5 to 0°C) and abundant annual total precipitation (~1300 mm). The landscape is largely dominated by black spruce (~80%) with a minor component of balsam fir (*Abies balsamea* [L.] Miller; ~15%) and white birch (*Betula papyrifera* Marshall; ~5%).

In Quebec, most boreal forests are managed through clearcut, in which all mature and commercial trees are harvested while protecting as much as possible the seedlings (< 1m height) and soils. Thus, it is possible to considerer that immediately after logging, the forest height is between < 1m and thereafter naturally regrowth through time. In our study area, about two-thirds of the landscape had been clearcut from 1955 to 2015 (Fig. 1). Between 5 and 20 years following clearcutting, approximately 25% of harvested stands were treated to precommercial thinning, a very common treatment in the boreal forest that reduces stand density and competing vegetation (Ashton and Kelty 2017). As is the case in most boreal forests, these stands are in remote areas that eventually are accessible only through very limited road networks a few years after harvesting because of rapid road network degradation. Deterioration of the road network limits access, thereby making post-harvest field-based monitoring problematic. These characteristics make our study area a very good case study for developing and evaluating our new proposed growth modeling approach for these northern forest ecosystems.

Dataset description

The airborne LiDAR dataset was acquired from two campaigns in 2012 and 2016, in which forests were overflown during or at the end of the growing season (June to November). About 77% of the study area had been surveyed in 2016 with an *Optech ALTM Galaxy* system and with a point density of 8.5 points.m^{-2}. Another important proportion of the study area (18 %) had been surveyed in 2012 with an *Optech ALTM 31000A* system and with a point density of 6.6 points.m^{-2}. Further details on the LiDAR acquisition campaigns can be found in the Appendix S1 (Table S1).

Raw point clouds were first classified into ground and non-ground returns using the *GroundFilter* algorithm provided in the *Fusion* software (McGaughey 2018). A digital terrain model (DTM) was then fitted to the ground returns to produce a 20 m resolution raster with the *GridSurfaceCreate* in *Fusion* (McGaughey 2018). The DTM was subtracted from the elevations of all non-ground returns to produce a normalized point cloud. Finally, a canopy height model (CHM; Fig. 1) was obtained by using the 95th percentile of point elevations of all non-ground returns (P95) in each 20 m × 20 m pixel, after removing returns < 1 m. P95 is frequently used to produce canopy height models (White et al. 2013), and exclusion of the lowest return (< 1 m) is usually applied to remove the returns from herbaceous-shrubby ground vegetation (Nyström et al. 2012).

The harvesting history (1955-2015) data were taken from forestry maps that are based on the interpretation of high resolution aerial photographs and from annual harvesting reports (MFFP 2018). The polygons are drawn at the 1:20,000 scale with a minimum size of 4 ha (see illustration in Fig. S1). The information contained in the polygons was transformed into a 20 m × 20 m raster, matching the CHM data resolution (Fig. 1). The age of the trees within each logged pixel was then calculated as the difference between LiDAR acquisition year and harvesting year. Between 5 and 20 years following clearcutting, 24% of harvested stands were treated to precommercial thinning. Consequently, we considered two distinct types of sylvicultural scenarios in our analysis: (1) clearcutting alone; and (2) clearcutting, followed by precommercial thinning.

Several additional environmental variables that could potentially influence forest height growth were also derived from LiDAR data or extracted from the forestry maps (Table 1). Slope, aspect and a topographic wetness index (TWI; Beven and Kirkby 1979) were derived from the LiDAR DTM raster. Elevation, slope and aspect were then combined with historical meteorological data (1981-2010) to compute the mean growing degree-day (GDD) per 20 m × 20 m pixel with

BIOSIM software (Régnière et al. 2014). Two categorical variables were extracted from modern forest maps (see illustration in Fig. S1): surface deposits (glacial, fluvio-glacial or rocky outcrops) and potential vegetation types. Potential vegetation types correspond to a fine scale level of Quebec's forest classification system that refers to the late-successional vegetation that would be expected under given environmental conditions (climate, physiography). In our study area, potential vegetation is represented by three major types: 1) balsam fir-black spruce forests (BF-BS); 2) balsam fir-paper birch forests (BF-PB), which are both found on rolling topography; and 3) black spruce-dominated forests on flat lands (BS).

We randomly sampled 20 m × 20 m pixels, where selected pixels must meet five conditions. First, because our analysis had focused on black spruce-dominated forests, only pixels with > 75% black spruce basal area, which was indicated in forest maps prior to clearcutting, were retained (MFFP 2018). Second, the first 50 m within the clearcut polygon boundaries were excluded to avoid border effects and stand margin delineation errors. Third, sampled pixels must be separated by a minimum distance of 250 m to avoid spatial autocorrelation (Matasci et al. 2018), the threshold of which was validated with a semi-variogram (Fig. S2; Curran 1988). Fourth, only stands that were aged ≥ 10-years-old after clearcutting were retained, given that trees < 10-years-old could be confused with ericaceous shrubs, which can reach > 1 m in height (Matasci et al. 2018). Maximum stand age after clearcutting was also limited to 53 years because too few pixels were older than that age. Fifth, the 1:20,000 polygons that identify clearcut areas had have a minimum size of 4 ha and could include small patches of remnant forest (i.e., individual pixels of 20 m × 20 m = 0.04 ha). To remove these patches from the analysis, we excluded pixels with aberrant heights for a given age since they were very likely associated with remnant forest patches. Aberrant height thresholds were defined using a database of > 65,000 black spruce trees, the age and height of which have been measured in the field through Quebec's network of permanent plots (MFFP 2016; Fig. S3). The maximum height threshold for a given age was defined as the 95th percentile of all field-based observations of tree height per age class. Applying these five conditions retained 3420 pixels that were subsequently allocated randomly to either a training set (2256 pixels; 66%) or a validation set (1164 pixels, 34%).

Modeling forest height growth

Preliminary analysis involved identifying pairs of environmental explanatory variables that were ambiguously correlated. Problematic correlations (Pearson $r > 0.5$) were found between stand age, elevation and degree-days (Fig. S4). This is not surprising since historically in this region, harvesting areas tended to progress over time from lower elevations in the southern part of our study area, to higher elevations located in the northern part (Fig. 1, Fig. S4). We decided to retain only stand age because it represented the most important gradient of values among these three variables for modeling forest height, which was confirmed by a generalized variance inflation factor analysis (Fox and Monette 1992; Appendix S1: Table S2).

We used a random forest model (Breiman 2001) to predict forest height growth since such machine learning approaches are very efficient in modeling non-linear ecological data with complex interactions (Christin et al. 2019). We trained the model using the *randomForest* function included in the *randomForest* package (version 4.6.14; Liaw and Wiener 2018) in the R statistical environment (R Core Team 2020). The training set (n = 2256) was analyzed to define optimal parameters using the *tuneRF* function, which was included in *randomForest* (Liaw and Wiener 2018). To evaluate the predictive power of our final model, we used our validation dataset (n = 1164) as a new input to the random forest model and compared observed and predicted values. We assessed the relative importance of variables in the model with the *importance* function of *randomForest*, which computes both the percentage increase in mean square error (%incMSE) and the increase in node purity for each explanatory variable (Liaw and Wiener 2018).

The model was finally used to produce maps of potential post-logging forest height growth across the whole landscape. For each 20 m × 20 m map pixels, we computed potential growth as the predicted height at 50 years, divided by 50, in order to obtain a map of height growth in cm.year^{-1} that is comparable with the results found in the literature. We also computed the model uncertainty using the quantile Random Forest regression approach (Meinshausen and Ridgeway 2006). In brief, the variance of predicted height values is quantified between the trees within the random forest model and used as a metric of prediction uncertainty. We used the *quantregForest* R package (Meinshausen 2017) to associate a standard deviation to each prediction (in cm.year^{-1}). The absolute standard deviation was then divided by the predicted height growth to obtain a relative standard deviation in percent.

Results

The comparison between observed and predicted pixel heights (i.e., LiDAR P95) from the validation dataset illustrates the strong predictive power of our random forest model (Fig. 2). The linear regression between predicted and observed values is very close to the theoretical relationship (1:1) and is strongly supported by several validation metrics (R^2 = 0.74, relative RMSE = 19%, and mean error = 0.003 m). The predictive power of our model was also consistent across age classes (Fig. S5).

Application of the two tests (%incMSE and increase in node purity) within the random forest analysis leads to a similar ordering for the first three variables in terms of their relative importance and are relatively coherent for the other ones (Fig. 2). We have chosen to rank the relative importance of variables based on %incMSE, which is generally considered as the most reliable metric (Strobl et al. 2007). Stand age emerges as a dominant variable for predicting forest height (Fig. 2). Topographic characteristics emerge as secondary variables (slope and TWI; Fig. 2), with best height growth on slopes with high TWI (i.e., low moisture) compared to lower slopes with high TWI (i.e., high moisture; Fig 3). Potential vegetation types rank fourth (Fig. 2), with better growth on BF-PB sites (balsam fir-paper birch on rolling topography), compared to BF-BS and BS sites (balsam fir-black spruce forests on rolling topography and black spruce-dominated forests on flat lands, respectively; Fig. 3). The type of silvicultural scenarios fifth (Fig. 2), with stands that have been treated to precommercial thinning showing slightly lower height growth compared to stands that have not been treated (Fig. 3). Surface deposits and aspect make the least important contributions in the model (Fig. 2); growth rates are generally higher on glacial surface deposits, while they are generally lower on western and southeastern exposures (i.e., aspect; Fig. 3).

Predicted forest height growth in the first 50 years after logging ranged between 15.7 and 27.2 cm.year^{-1} across the whole study area (Fig. 4), with a mean of 20.5 cm.year^{-1}. The spatial patterns of potential height growth were strongly linked to the effect of topographical variables described above. These predictions were associated with uncertainties comprised between 17.6 and 34.3 %, and with a mean of 24.1 %.

Discussion and conclusion

Our first objective was to evaluate the potential of an approach combining a single airborne LiDAR acquisition with time-since-harvesting maps to model forest height growth of post-logged boreal forests. Overall, our results highlight the strong power of this approach: we were able to predict ≈75% of the validation dataset variation in stand height, with a relative RMSE inferior to 20%. Predicted forest height growth rates for the first 50 years after logging ranged between 16 and 27 cm.year^{-1} across the whole study area. These results are highly consistent with the height growth rates found in boreal forests of Canada and the northeastern US with either field-based (Béland and Bergeron 1996, Gutsell and Johnson 2002, Oboite and Comeau 2019) or remote-sensed data (Dolan et al. 2009, Neigh et al. 2016). Additionally, we used 59 permanent plots in a 20 km radius of our study area to compare our results with filed-based data. The height growth rates observed in individual black spruces remeasured between 1974 and 2015, and aged between 10 and 50 years, were also highly consistent with the results of our model (observed growth rates comprised between 8.3 cm.year^{-1} and 34.5 cm.year^{-1}; Table S3).

Our model revealed an important ecological gradient that is responsible for differences in forest height growth at the landscape scale. Slope and site moisture (TWI) emerged as the second and third most important explanatory variables, after stand age. Best growth occurred on moderate slopes with low soil moisture compared to lower slopes with high soil moisture. This is not surprising since moist lower slopes are generally associated with poor drainage and high accumulations of organic matter that strongly limit forest productivity (Lavoie et al. 2007, Laamrani et al. 2014). Similarly, better growth rates were found on balsam fir-paper birch potential vegetation types (BF-PB) and glacial surface deposits that are likely associated with this drainage and organic matter gradient, given that these sites are generally associated with best drainage conditions and fertility. Our model's integration of environmental variables represents a major advancement compared to previous studies using time-since disturbance and remote-sensed data to model forest growth. These studies were restricted to estimates the growth or productivity observed on sites that comprised both time-since disturbance and remote-sensed height data (Dolan et al. 2009, Tompalski et al. 2015, Neigh et al. 2016). Our model goes further since, once trained, it can predict forest growth on other sites based on their environmental characteristics.

Our results also highlighted the potential of our method to model the effects of different stand-replacing disturbance types on forest height growth. Precommercial thinning following clearcutting had a small negative effect on height growth when compared to other stands, which could be linked to several mechanisms. First, although we made efforts to limit our analyses to black spruce-dominated stands (> 75% of the basal area), the presence of a minor deciduous component is ubiquitous in our data (Fig. S6). These thinned individuals include mostly *Betula papyrifera,* and to a lesser extent, trembling aspen (*Populus tremuloides*). The lower heights that were observed in precommercial thinning scenarios may thus be linked to the goal of precommercial thinning, which removes fast-growing deciduous species that overtop black spruce or balsam fir stems. Indeed, a lower proportion of deciduous components are encountered in thinned stands (Fig. S6).

Our method combines airborne LiDAR and historical stand-replacing disturbance maps and, thus, provides a very simple and powerful tool to model young forest growth to any forest worldwide that is affected by stand-replacing disturbances (e.g., clearcuts, fire, windthrow, agricultural land abandonment; Curtis et al. 2018). Such data are becoming available at the global scale with space-borne LiDAR forest structure and aboveground biomass data (Hancock et al. 2019), together with remote-sensed historical forest disturbance areas (Hansen et al. 2013) and types (Guindon et al. 2017, 2018, Curtis et al. 2018). As an advantage over most standard growth models, our method uses landscape-scale environmental variables to accurately predict forest productivity with a high spatial resolution and over large extents. Such model outcomes can be used for the forest industry to maintain forest ecosystem services by adjusting the harvesting rates depending on forest productivity across the landscapes. Moreover, applying this method to larger extents would allow improved models by integrating the regional climate gradients (i.e., temperature, moisture) as predictor variables. Such improved models could allow to project the effect of future climate change upon forest productivity over a wide range of different site characteristics and thus help to adjust harvesting rates or predict future forest carbon storage.

Acknowledgements

This project was financially supported by the Quebec Ministère des Forêts de la Faune et des Parcs (MFFP) project #142332166 to Y. Boucher and the Collaborative Research and Development program of the Natural Sciences and Engineering Research Council (NSERC grant # RDCPJ 508853-17). We are grateful to our industrial partners: Ryam, Produits forestiers résolu, Rébec, Barrette-Chapais, and Rival solutions This research could not have been performed without the collaboration of J.F. Bourdon (MFFP) for the availability of high-quality datasets (forest plots and LiDAR) and his support of the data analysis. Also, we wish to thank J. Noël and I. Auger of the MFFP for their support related to the statistical analysis, Philippe Villemaire and Rémi St-Amand of Natural Resources Canada for the availability and analysis of several explanatory variables and W.F.J. Parsons for the English revision. We finally thanks Osvaldo Valeria and three anonymous reviewers for their constructive feedbacks on previous version of the manuscript.

References

Ashton, M. S., and M. J. Kelty. 2017. The practice of silviculture: applied forest ecology. 10th edition. Wiley, Hoboken, NJ.

Béland, M., and Y. Bergeron. 1996. Height growth of jack pine (*Pinus hanksiana*) in relation to site types in boreal forests of Abitibi, Quebec. Canadian Journal of Forest Research 26:2170–2179.

Beven, K. J., and M. J. Kirkby. 1979. A physically based, variable contributing area model of basin hydrology. Hydrological Sciences Bulletin 24:43–69.

Boisvenue, C., and S. W. Running. 2006. Impacts of climate change on natural forest productivity - evidence since the middle of the 20th century. Global Change Biology 12:862–882.

Boucher, Y., M. Perrault-Hébert, R. Fournier, P. Drapeau, and I. Auger. 2017. Cumulative patterns of logging and fire (1940–2009): consequences on the structure of the eastern Canadian boreal forest. Landscape Ecology 32:361–375.

Breiman, L. 2001. Random forests. Machine learning 45:5–32.

Cao, L., N. C. Coops, J. L. Innes, S. R. J. Sheppard, L. Fu, H. Ruan, and G. She. 2016. Estimation of forest biomass dynamics in subtropical forests using multi-temporal airborne LiDAR data. Remote Sensing of Environment 178:158–171.

Christin, S., É. Hervet, and N. Lecomte. 2019. Applications for deep learning in ecology. Methods in Ecology and Evolution 10:1632–1644.

Cook-Patton, S. C., S. M. Leavitt, D. Gibbs, N. L. Harris, K. Lister, K. J. Anderson-Teixeira, R. D. Briggs, R. L. Chazdon, T. W. Crowther, P. W. Ellis, H. P. Griscom, V. Herrmann, K. D. Holl, R. A. Houghton, C. Larrosa, G. Lomax, R. Lucas, P. Madsen, Y. Malhi, A. Paquette, J. D. Parker, K. Paul, D. Routh, S. Roxburgh, S. Saatchi, J. van den Hoogen, W. S. Walker, C. E. Wheeler, S. A. Wood, L. Xu, and B. W. Griscom. 2020. Mapping carbon accumulation potential from global natural forest regrowth. Nature 585:545–550.

Curran, P. J. 1988. The semivariogram in remote sensing: An introduction. Remote Sensing of Environment 24:493–507.

Curtis, P. G., C. M. Slay, N. L. Harris, A. Tyukavina, and M. C. Hansen. 2018. Classifying drivers of global forest loss. Science 361:1108–1111.

Dolan, K., J. G. Masek, C. Huang, and G. Sun. 2009. Regional forest growth rates measured by combining ICESat GLAS and Landsat data. Journal of Geophysical Research: Biogeosciences 114.

D'Orangeville, L., D. Houle, L. Duchesne, R. P. Phillips, Y. Bergeron, and D. Kneeshaw. 2018. Beneficial effects of climate warming on boreal tree growth may be transitory. Nature Communications 9.

Fox, J., and G. Monette. 1992. Generalized collinearity diagnostics. Journal of the American Statistical Association 87:178–183.

Guindon, L., P. Bernier, S. Gauthier, G. Stinson, P. Villemaire, and A. Beaudoin. 2018. Missing forest cover gains in boreal forests explained. Ecosphere 9.

Guindon, L., P. Villemaire, R. St-Amant, P. Y. Bernier, A. Beaudoin, F. Caron, M. Bonucelli, and H. Dorion. 2017. Canada Landsat Disturbance (CanLaD): a Canada-wide Landsat-based 30-m resolution product of fire and harvest detection and attribution since 1984. Natural Resources Canada.

Gutsell, S. L., and E. A. Johnson. 2002. Accurately ageing trees and examining their height-growth rates: implications for interpreting forest dynamics. Journal of Ecology 90:153–166.

Hancock, S., J. Armston, M. Hofton, X. Sun, H. Tang, L. I. Duncanson, J. R. Kellner, and R. Dubayah. 2019. The GEDI simulator: A large-footprint waveform lidar simulator for calibration and validation of spaceborne missions. Earth and Space Science:2018EA000506.

Hansen, M. C., P. V. Potapov, R. Moore, M. Hancher, S. A. Turubanova, A. Tyukavina, D. Thau, S. V. Stehman, S. J. Goetz, T. R. Loveland, A. Kommareddy, A. Egorov, L. Chini, C. O. Justice, and J. R. G. Townshend. 2013. High-Resolution Global Maps of 21st-Century Forest Cover Change. Science 342:850–853.

Huang, J., J. C. Tardif, Y. Bergeron, B. Denneler, F. Berninger, and M. P. Girardin. 2010. Radial growth response of four dominant boreal tree species to climate along a latitudinal gradient in the eastern Canadian boreal forest. Global Change Biology 16:711–731.

Laamrani, A., O. Valeria, Y. Bergeron, N. Fenton, L. Z. Cheng, and K. Anyomi. 2014. Effects of topography and thickness of organic layer on productivity of black spruce boreal forests of the Canadian Clay Belt region. Forest Ecology and Management 330:144–157.

Lavoie, M., K. Harper, D. Paré, and Y. Bergeron. 2007. Spatial pattern in the organic layer and tree growth: A case study from regenerating *Picea mariana* stands prone to paludification. Journal of Vegetation Science 18:213–222.

Lefsky, M. A., D. P. Turner, M. Guzy, and W. B. Cohen. 2005. Combining lidar estimates of aboveground biomass and Landsat estimates of stand age for spatially extensive validation of modeled forest productivity. Remote Sensing of Environment 95:549–558.

Liaw, A., and M. Wiener. 2018. randomForest: Breiman and Cutler’s Random Forests for Classification and Regression.

Lindenmayer, D. B., M. J. Westgate, B. C. Scheele, C. N. Foster, and D. P. Blair. 2019. Key perspectives on early successional forests subject to stand-replacing disturbances. Forest Ecology and Management 454:117656.

Matasci, G., T. Hermosilla, M. A. Wulder, J. C. White, N. C. Coops, G. W. Hobart, D. K. Bolton, P. Tompalski, and C. W. Bater. 2018. Three decades of forest structural dynamics over Canada’s forested ecosystems using Landsat time-series and lidar plots. Remote Sensing of Environment 216:697–714.

McDowell, N. G., C. D. Allen, K. Anderson-Teixeira, B. H. Aukema, B. Bond-Lamberty, L. Chini, J. S. Clark, M. Dietze, C. Grossiord, A. Hanbury-Brown, G. C. Hurtt, R. B. Jackson, D. J. Johnson, L. Kueppers, J. W. Lichstein, K. Ogle, B. Poulter, T. A. M. Pugh, R. Seidl, M. G.

Turner, M. Uriarte, A. P. Walker, and C. Xu. 2020. Pervasive shifts in forest dynamics in a changing world. Science 368:eaaz9463.

McGaughey, R. 2018. FUSION/LDV: Software for LiDAR data analysis and visualization - V3.10. USDA Forest Service.

Meinshausen, N. 2017. quantregForest: Quantile Regression Forests.

Meinshausen, N., and G. Ridgeway. 2006. Quantile regression forests. Journal of Machine Learning Research 7.

Meyer, V., S. S. Saatchi, J. Chave, J. W. Dalling, S. Bohlman, G. A. Fricker, C. Robinson, M. Neumann, and S. Hubbell. 2013. Detecting tropical forest biomass dynamics from repeated airborne lidar measurements. Biogeosciences 10:5421–5438.

MFFP. 2016. Placettes-échantillons permanentes: normes techniques. Ministère des Forêts, de la Faune et des Parcs, Secteur des forêts, Direction des inventaires forestiers.

MFFP. 2018. Cartographie du 5e inventaire écoforestier du Québec méridional: méthodes et données associées. Ministère des Forêts, de la Faune et des Parcs, Secteur des forêts, Direction des inventaires forestiers.

Næsset, E., T. Gobakken, O. M. Bollandsås, T. G. Gregoire, R. Nelson, and G. Ståhl. 2013. Comparison of precision of biomass estimates in regional field sample surveys and airborne LiDAR-assisted surveys in Hedmark County, Norway. Remote Sensing of Environment 130:108–120.

Neigh, C. S. R., J. G. Masek, P. Bourget, K. Rishmawi, F. Zhao, C. Huang, B. D. Cook, and R. F. Nelson. 2016. Regional rates of young US forest growth estimated from annual Landsat disturbance history and IKONOS stereo imagery. Remote Sensing of Environment 173:282–293.

Nicklen, E. F., C. A. Roland, R. W. Ruess, J. H. Schmidt, and A. H. Lloyd. 2016. Local site conditions drive climate-growth responses of *Picea mariana* and *Picea glauca* in interior Alaska. Ecosphere 7:e01507.

Nyström, M., J. Holmgren, and H. Olsson. 2012. Prediction of tree biomass in the forest–tundra ecotone using airborne laser scanning. Remote Sensing of Environment 123:271–279.

Oboite, F. O., and P. G. Comeau. 2019. Competition and climate influence growth of black spruce in western boreal forests. Forest Ecology and Management 443:84–94.

Pflugmacher, D., W. B. Cohen, R. E. Kennedy, and Z. Yang. 2014. Using Landsat-derived disturbance and recovery history and lidar to map forest biomass dynamics. Remote Sensing of Environment 151:124–137.

Pretzsch, H., P. Biber, G. Schütze, and K. Bielak. 2014. Changes of forest stand dynamics in Europe. Facts from long-term observational plots and their relevance for forest ecology and management. Forest Ecology and Management 316:65–77.

R Core Team. 2020. R: A Language and Environment for Statistical Computing. R Foundation for Statistical Computing, Vienna, Austria.

Régnière, J., R. Saint-Amant, and A. Béchard. 2014. BioSIM 10: user's manual. Page (Laurentian Forestry Centre, Ed.).

Ryan, M. G., D. Binkley, J. H. Fownes, C. P. Giardina, and R. S. Senock. 2004. An experimental test of the causes of forest growth decline with stand age. Ecological Monographs 74:393–414.

Strobl, C., A.-L. Boulesteix, A. Zeileis, and T. Hothorn. 2007. Bias in random forest variable importance measures: Illustrations, sources and a solution. BMC Bioinformatics 8:25.

Tompalski, P., N. C. Coops, J. C. White, T. R. H. Goodbody, C. R. Hennigar, M. A. Wulder, J. Socha, and M. E. Woods. 2021. Estimating Changes in Forest Attributes and Enhancing Growth Projections: a Review of Existing Approaches and Future Directions Using Airborne 3D Point Cloud Data. Current Forestry Reports.

Tompalski, P., N. C. Coops, J. C. White, M. A. Wulder, and P. D. Pickell. 2015. Estimating Forest Site Productivity Using Airborne Laser Scanning Data and Landsat Time Series. Canadian Journal of Remote Sensing 41:232–245.

Vanclay, J. K., and J. P. Skovsgaard. 1997. Evaluating forest growth models. Ecological Modelling 98:1–12.

Weiskittel, A. R., D. W. Hann, J. A. Kershaw, and J. K. Vanclay. 2011. Forest growth and yield modeling. John Wiley & Sons, Ltd, Chichester, UK.

White, J., Canadian Forest Service, and Canadian Wood Fibre Centre. 2013. A best practices guide for generating forest inventory attributes from airborne laser scanning data using the area-based approach.

Table 1. Description of variable sources, type (Cont., continuous; Categ., categorical), and range in the training and validation datasets. LiDAR-derived data are 20 m × 20 m rasters, and data derived from forestry maps are 1:20000 polygons with a minimum polygon size of 4 ha (see Fig. S1 for a visual illustration). The first number is the mean value in the range column of continuous variables, while numbers within parentheses are minimum and maximum.

Variables	Source	Type (unit)	Range
Stand height (P95)	LiDAR	Cont. (m)	6.04 (1.79 - 16.19)
Stand age	Forestry maps	Cont. (year)	29.15 (10 - 53)
Elevation	LiDAR	Cont. (m a.s.l.)	460 (130 - 700)
Slope	LiDAR	Cont. (°)	7.82 (0.01 - 28.49)
TWI	LiDAR	Cont. (no unit)	6.26 (3.31 - 14.79)
Aspect	LiDAR	Categ.	N, NE, E, SE, S, SO, O, NO
Degree-days	Meteorological	Cont. (°C)	1123 (990 - 1289)
Sylvicultural scenarios	Forestry maps	Categ.	Clearcut, Clearcut + thinning
Potential vegetation	Forestry maps	Categ.	BF-BS, BF-PB, BS
Surface deposit	Forestry maps	Categ.	Glacial, fluvio-glacial, rocky

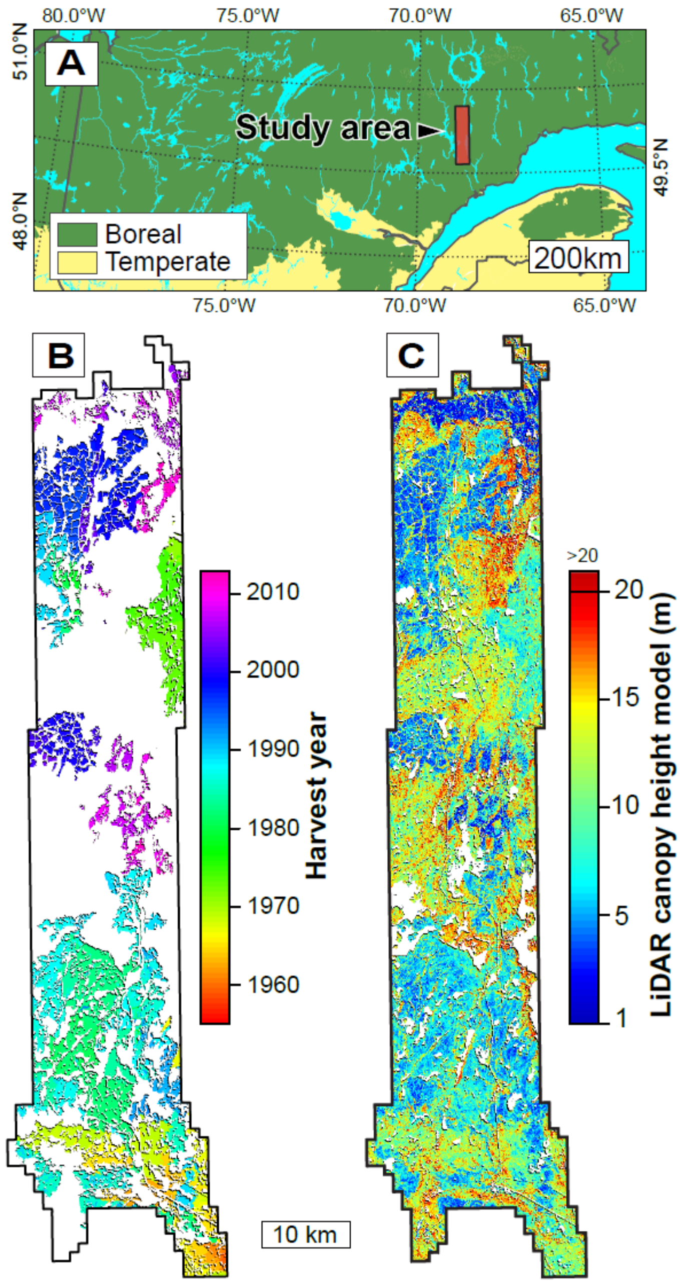

Figure 1. (A) Location of the study area in the boreal forest of eastern Canada. (B) a 20 m × 20 m raster layer of historical harvesting, and (C) the canopy height model based on airborne LiDAR data (2012 to 2016). Note that pixels > 20 m in (C) are displayed in dark red.

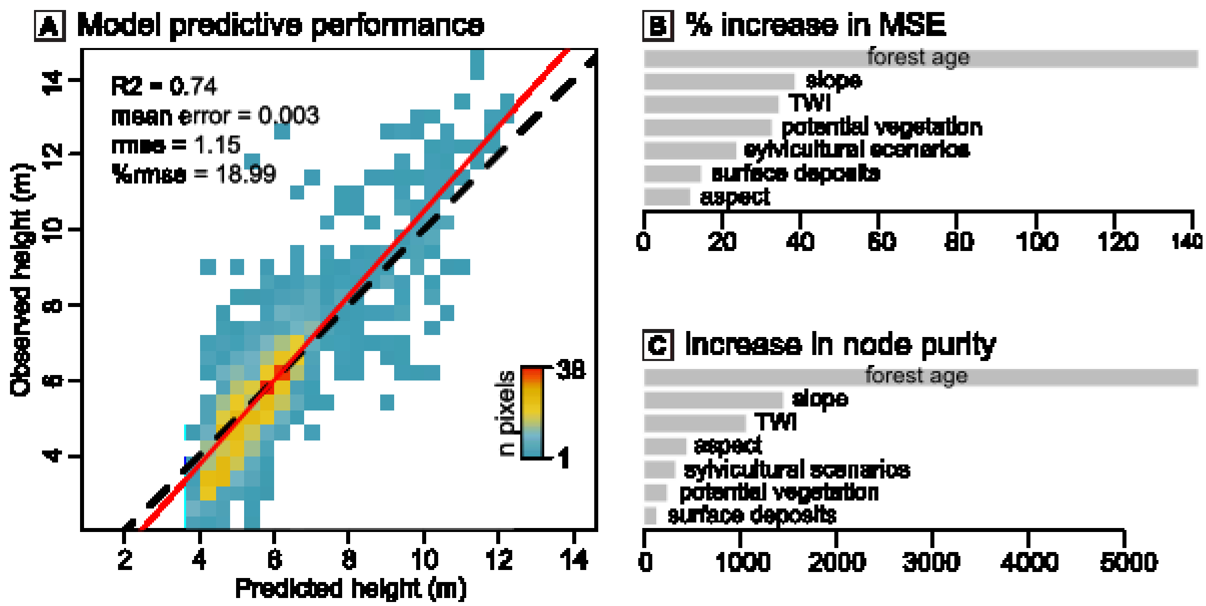

Figure 2. (A) Random forest model evaluation and (B, C) variable importance. Model predictive power was assessed in (A) through the comparison between observed and predicted pixel heights in the validation dataset (n = 1164 pixels). Point cloud density is displayed as a color gradient. The dotted black line shows the 1:1 theoretical relationship, while the solid red line shows the relationship modeled through ordinary least-squares regression. Variable importance in the random forest model was assessed (A) by percent increase in mean-square error and (B) by increase in node purity.

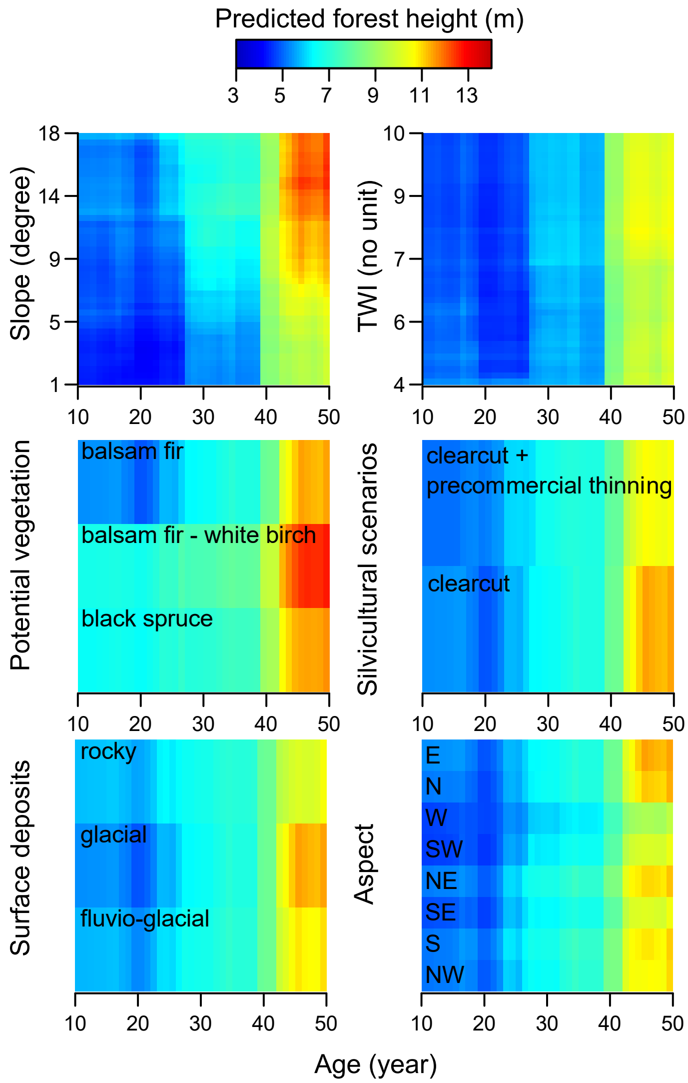

Figure 3. Interactive effects of stand age with other variables on forest height. For each variable, plots show the predicted forest height across the observed range of this variable, with other continuous variables held at median values (except for slope, which was held at 15° for categorical variable plots, to depict their effects in the best growing conditions). Categorical variables were held at the most common category across the training dataset (i.e., eastern exposure, clearcut silvicultural scenario, balsam fir potential vegetation, and glacial surface deposit). Ranges of slope and TWI were defined by their respective 2.5 and 97.5 percentiles.

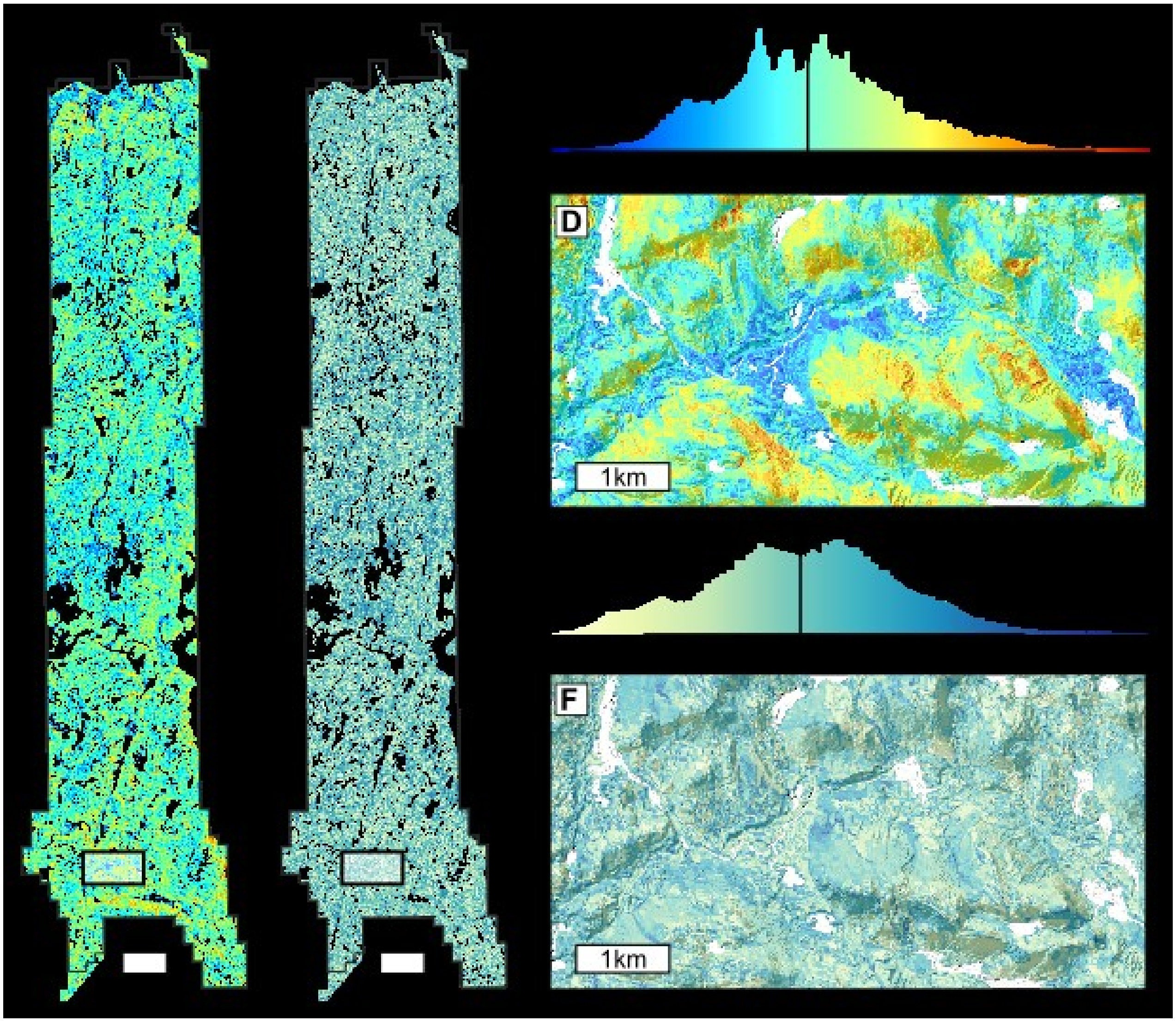

Figure 4. Predicted potential post-logging height growth in the first 50 years after logging and uncertainty across the whole study area (maps A, B and histograms C, E) and for a selected portion of the landscape (D, F). All maps are displayed on the same color scales shown in histograms, and vertical bar in histograms show the mean value across the whole study area. The black rectangles at the bottom of maps A and B show the location of D and F. Shaded reliefs were added to maps D and F to depict the strong variation in growth rates across the topographical gradient. Predictions were made using the clearcutting alone sylvicultural scenario (i.e., no pre-commercial thinning).